**Supplementary Information**

**A Fentanyl Assay Derived from Intermolecular Interaction Enabled Small Molecule Recognition (iMSR) with Differential Impedance Analysis for Point-of-Care Testing**

*Zhe Wang[1*], Amit Nautiyal[2], Christopher Alexopoulos[1], Rania Aqrawi[1], Xiaozhou Huang[3], Ashraf Ali[4], Katherine E. Lawson[4], Kevin Riley[2], Andrew J. Adamczyk[4], Pei Dong[3], Xinyu Zhang[4]*

[1] Chemistry Department, Oakland University, Rochester, MI 48309 USA

[2] Department of Chemistry, Xavier University of Louisiana, New Orleans, LA 70125 USA

[3] Department of Mechanical Engineering, George Mason University, Fairfax, VA 22030 USA

[4] Department of Chemical Engineering, Auburn University, Auburn, AL 36849 USA
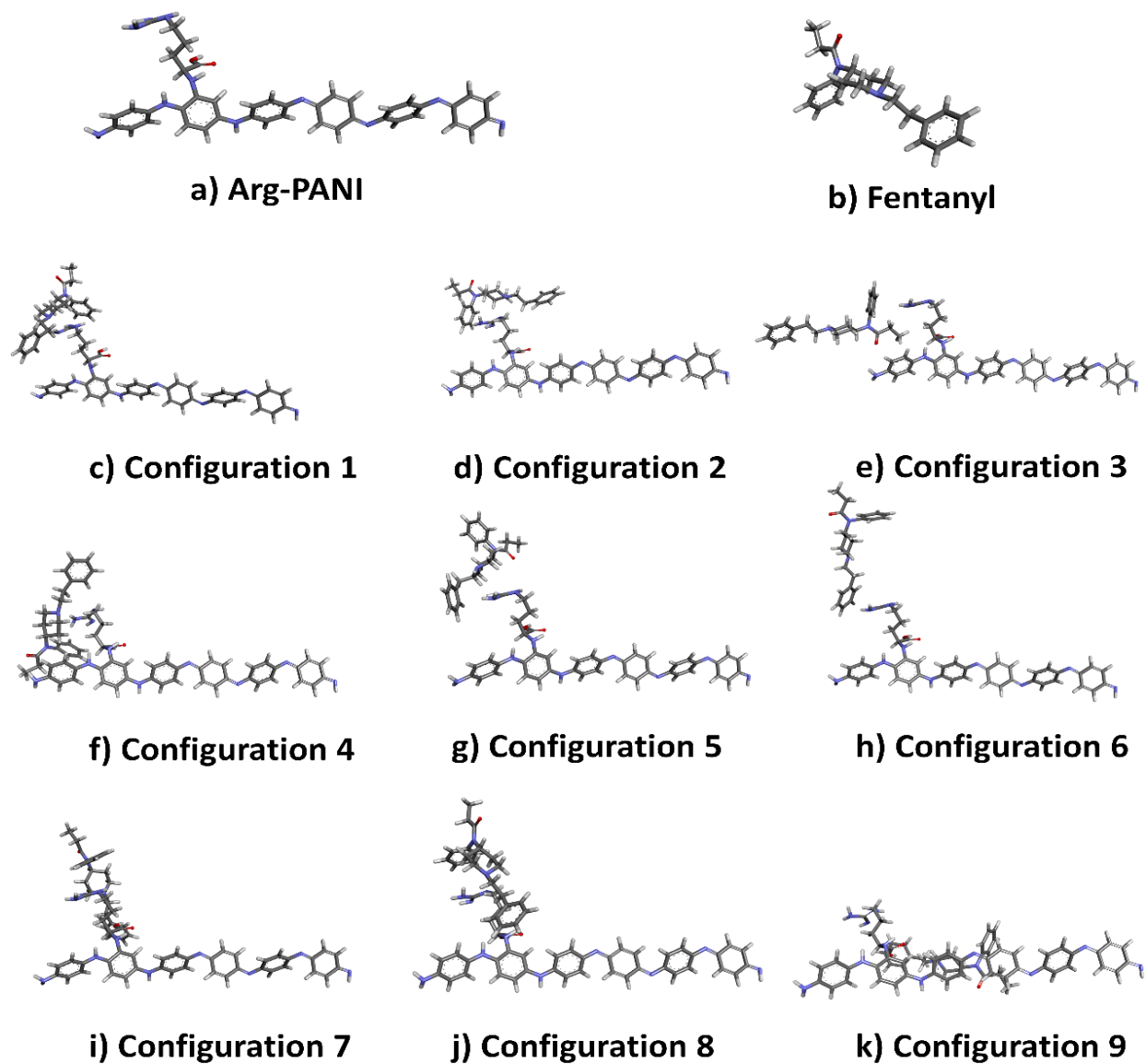
**Table of Contents**

**SI-1. Computational Methodology Supporting Information.**

The interaction between arginine bound polyaniline and fentanyl has been investigated with quantum chemical methods using density functional theory (DFT) with an empirical dispersion correction[1-3]. The adsorption complexes of various configurations of fentanyl (adsorbate) and arginine substituted polyaniline hexamer (AS-PANI) (adsorbent), representing the sensor surface, were investigated utilizing Density Functional Theory (DFT) calculations as implemented in the Gaussian 16 software[3]. The generalized gradient approximation (GGA) with the Becke/Lee, Yang and Parr (BLYP) exchange correlation functional has been used with 6-31G(d) basis set[1, 2, 4]. The Grimme dispersion with the original D3 damping function was used to provide an improved description of the nonlocal nature of the electron correlation, particularly hydrogen bonds and van der Waals interactions[5]. Implicit solvation using a self-consistent reaction field (SCRF) with the Conductor-like Polarizable Continuum Model (CPCM) was employed with the dielectric constant of water ($\varepsilon=78$)[6]. A total of 36 complex configurations of fentanyl and AS-PANI have been investigated. The four isomers of AS-PANI were studied which included three zwitterionic isomers of the arginine side chain and one isomer without a zwitterion (Figure S4). The amino acid side chain of arginine consists of a 3-carbon aliphatic straight chain, the distal end of which is capped by a guanidino group, which has a pKa of 12.48. At physiological pH, the carboxylic acid is deprotonated to a carboxylate group ($-COO^-$) and the guanidino group is protonated to give the guanidinium forms [*Zwitterion 1*: $(-N^+H_2-C(-NH_2)(=NH)$, *Zwitterion 2*: $-NH-C(-NH_2)(=N^+H_2)$, *Zwitterion 3*: $-NH-C(-N^+H_3)(=NH)$]. Guanidinium groups present in conductive polymers such as PANI induce their charge transport through complex formation with fentanyl. Thus, sensor properties are likely to be directly correlated to the number of guanidinium groups present and accessible to complex formation on the conductive polymer backbone. The total intermolecular interaction between the arginine substituted polyaniline (AS-PANI) and fentanyl can be categorized into multiple noncovalent interactions, such as hydrogen bonding between the hydrogen of the guanidino group of arginine and the nitrogen of fentanyl, as well as various polar-π, cation-π & π-π interactions, and dispersion forces. Depending on the various

configurations and the zwitterionic state of complex, calculated binding (or adsorption) energies of fentanyl

and AS-PANI varied from -0.38 eV to -2.38 eV with a mean value of -1.19 eV (Tables S1 and S2).
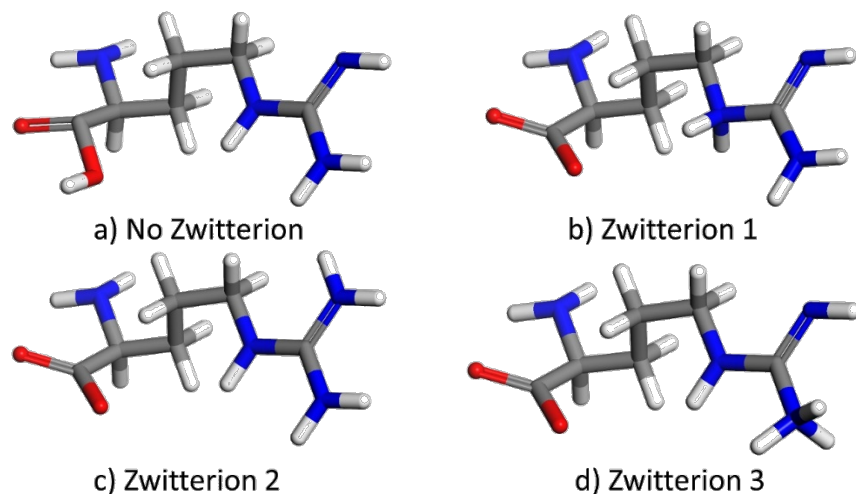


Figure S1. Four zwitterionic isomers of Arginine a) no zwitterion where carboxylic acid and guanidino

groups remain unionized, and b) to d) showing zwitterionic structures of arginine with a negatively charged

carboxylate group and a positively charged guanidinium group. The differences between the three

zwitterionic states are due to the protonation of the three different nitrogen atoms of the guanidino group.

**a) Arg-PANI**

**b) Fentanyl**

**c) Configuration 1**

**d) Configuration 2**

**e) Configuration 3**

**f) Configuration 4**

**g) Configuration 5**

**h) Configuration 6**

**i) Configuration 7**

**j) Configuration 8**

**k) Configuration 9**

**Figure S2. Optimized geometries** of a) arginine substituted polyaniline (AS-PANI), b) Fentanyl, and c) to k) various adsorption complex configurations of fentanyl and AS-PANI. All optimized geometries shown are the non-zwitterionic isomers of AS-PANI.

The nine fentanyl and sensor (AS-PANI) complex configurations with lowest interaction energies were shown in Figure S5. All these complexes were stabilized by multiple hydrogen, cation/anion-π interactions, π-π interactions, or N-H---π interactions between fentanyl and AS-PANI in each of the configurations. The interaction between fentanyl and AS-PANI showed significantly weaker binding energies when the interacting functional groups of fentanyl were kept at a distance from the sensor (configurations 5 and 6). In both the configurations, the complexes are stabilized by N-H---π interactions. On the other hand, when these functional groups were in proximity of a guanidino group and aromatic rings, the binding energies increased significantly. In configuration 8, the complex is stabilized by $N^+$-H---π, H-bond between the N of piperidine and the guanidino group, and π-π interactions, whereas in the configuration 9, it is stabilized by π-π interactions between PANI backbone and fentanyl. The configurations 1, 2, and 4 were stabilized by H-bonding between the N of piperidine and the guanidino group along with $N^+$-H---π and N-H---π interactions between PANI linkage and π-bonding of phenylethyl (configuration 1), as well as π-π interactions and C=O---H-N between PANI and fentanyl (configuration 2, 4).

Noncovalent binding (or adsorption) energies ($E_{Binding}$) for various configurations of Fentanyl complexed to an arginine-bound polyaniline hexamer have been calculated using equation below:

$$E_{Binding} = E_{Cluster} - (E_{PANI-Arg} + E_{Fentanyl})$$

Where $E_{Cluster}$ is the total electronic energy of the complex (fentanyl and AS-PANI), $E_{Fentanyl}$ is the electronic energy of a fentanyl molecule, and $E_{AS-PANI}$ is the electronic energy of the arginine substituted polyaniline (AS-PANI). Our group has implemented similar model systems to predict key phenomena such as electronic properties, adsorption energies, and charge transfer phenomena in various materials and composites[7-9].

**Table S1. The calculated binding energy values for all adsorption complex configurations**. All fentanyl and substituted polyaniline hexamer (AS-PANI). [No Zwitterion: arginine and carboxylic acid, Zwitterion 1: (-$N^+H_2$-C(-$NH_2$)(=NH), Zwitterion 2: -NH-C(-$NH_2$)(=$N^+H_2$), Zwitterion 3: -NH-C(-$N^+H_3$)(=NH)]

| Configuration Number | Binding Energy (eV) | | | |
| --- | --- | --- | --- | --- |
| | AS-PANI Isomers | | | |
| | No Zwitterion | Zwitterion 1 | Zwitterion 2 | Zwitterion 3 |
| 1 | -0.961 | -1.227 | -0.795 | -2.029 |
| 2 | -1.426 | -1.959 | -0.915 | -1.310 |
| 3 | -0.911 | -1.226 | -0.730 | -0.839 |
| 4 | -1.426 | -1.564 | -1.461 | -2.102 |
| 5 | -0.641 | -0.848 | -0.705 | -0.746 |
| 6 | -0.380 | -1.250 | -0.393 | -0.669 |
| 7 | -0.911 | -1.321 | -1.350 | -1.120 |
| 8 | -1.435 | -1.314 | -1.222 | -2.378 |
| 9 | -1.257 | -1.333 | -1.181 | -1.503 |

**Table S2. Summary statistics for calculated binding energy values**. All adsorption complex configurations of fentanyl and arginine substituted polyaniline hexamer (AS-PANI).

| Statistics Estimators | AS-PANI Isomers | | | | |
| --- | --- | --- | --- | --- | --- |
| | All Data | No Zwitterion | Zwitterion 1 | Zwitterion 2 | Zwitterion 3 |
| Mean (eV) | -1.19 | -1.039 | -1.338 | -0.973 | -1.411 |
| Standard Error (eV) | 0.076 | 0.126 | 0.099 | 0.117 | 0.211 |
| Median (eV) | -1.226 | -0.961 | -1.314 | -0.915 | -1.310 |
| Standard Deviation (eV) | 0.457 | 0.377 | 0.298 | 0.351 | 0.634 |
| Sample Variance (eV) | 0.209 | 0.142 | 0.089 | 0.123 | 0.402 |
| Kurtosis | 0.437 | -0.772 | 2.538 | -0.963 | -1.489 |
| Skewness | -0.562 | 0.494 | -0.789 | 0.143 | -0.352 |
| Range (eV) | 1.9982 | 1.0555 | 1.11164 | 1.0678 | 1.70921 |
| Minimum (eV) | -2.378 | -1.435 | -1.959 | -1.461 | -2.378 |
| Maximum (eV) | -0.380 | -0.380 | -0.848 | -0.393 | -0.669 |
| 95% Confidence Level (eV) | 0.155 | 0.290 | 0.229 | 0.270 | 0.488 |

The statistical comparison among the forms with and without zwitterions using one-way ANOVA (Table S3) showed that mean values of binding energies of the four isomer forms of the AS-PANI are not significantly different, i.e., F< F critical and p-value > 0.05 or 0.1. Figure S4 and Table S3 provide detailed statistical analysis of the variance between groups and within groups, where groups for our study are defined as the different isomers of the AS-PANI.

**Table S3. One-way Analysis of Variance (ANOVA) of calculated binding energy values.** ($\alpha$=0.05).

| Source of Variation | Sum of Squares | Degrees of Freedom | Mean Sum of Squares | F-value | P-value | F-critical |
|---|---|---|---|---|---|---|
| **Between Groups** | 1.267 | 3 | 0.422 | | | |
| **Within Groups** | 6.054 | 32 | 0.189 | 2.232 | 0.103 | 2.901 |
| **Total** | 7.320 | 35 | | | | |

**Figure S3. The calculated binding energy values for all adsorption complex configurations**.

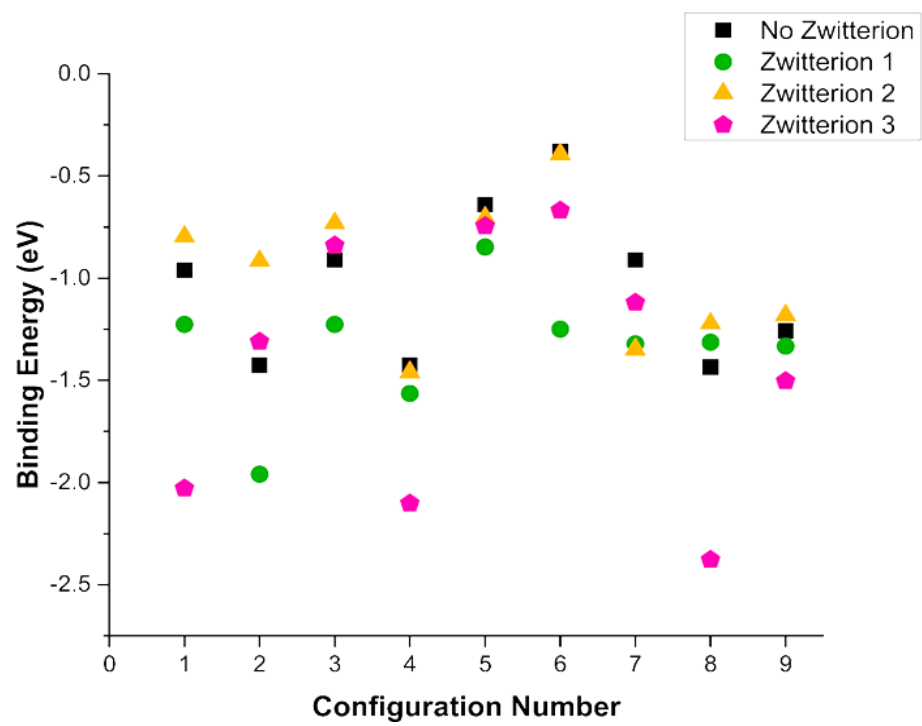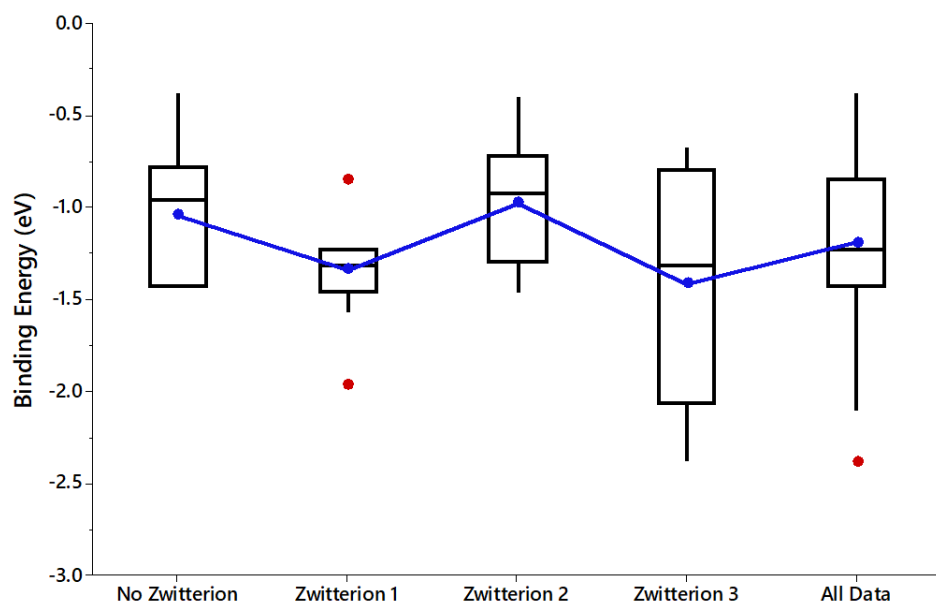**Figure S4. Box and whisker plots for calculated binding energy values for all adsorption complex configurations.** All fentanyl and substituted polyaniline hexamer (AS-PANI). Mean binding energy values for all isomer forms are in blue color, and outliers are in red color.

**SI-2. Experimental Methodology Supporting Information**

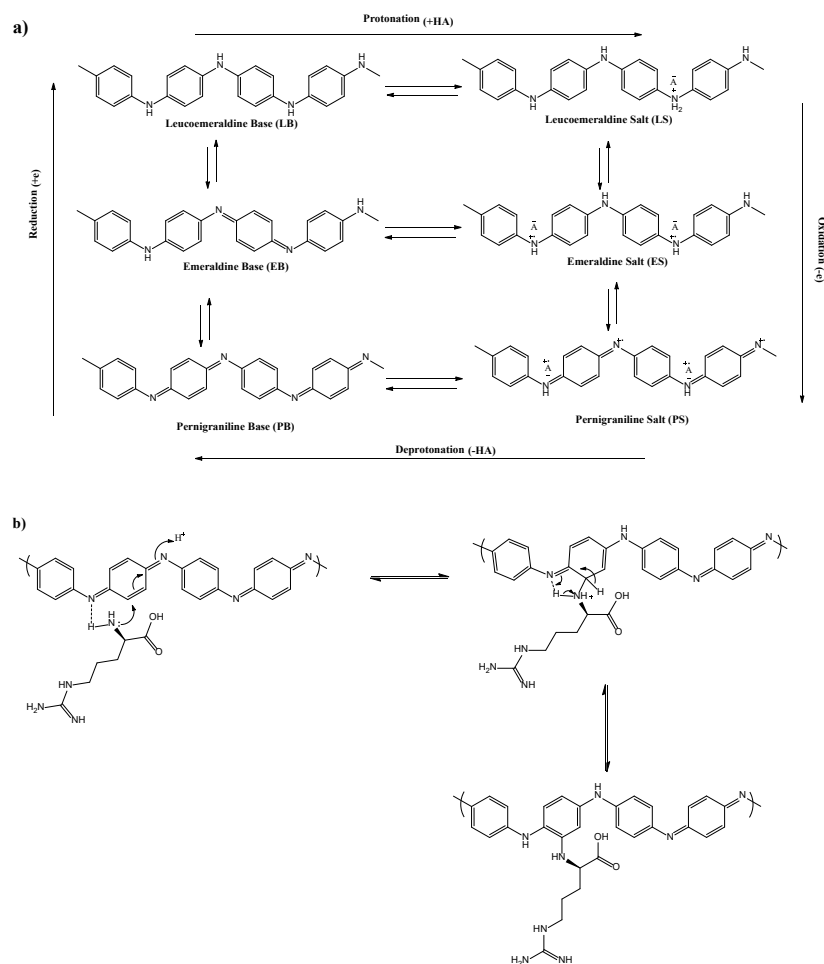**PANI structure and Functionalization.** Typically, polyaniline shows transformation of its three different oxidation states (L, E, P) during cyclic voltammetry in strongly acidic electrolyte. This change in oxidation states can be seen in voltammogram as redox peaks in positive or negative scan[10]. On applying 1V to polyaniline, the polymer quickly transforms to fully oxidized state (pernigraniline). This allows nucleophilic addition of arginine on quinoid structure of polyaniline.



**Figure S5. PANI structure and functionalization** (a) The scheme representing structure and three oxidation states of polyaniline and their doping and de-doping process. (b) The mechanism for the addition of functional arginine to the quinoid unit of polyaniline.

**SI-3. Sensor Characterizations.**

a)



b)



c)



d)
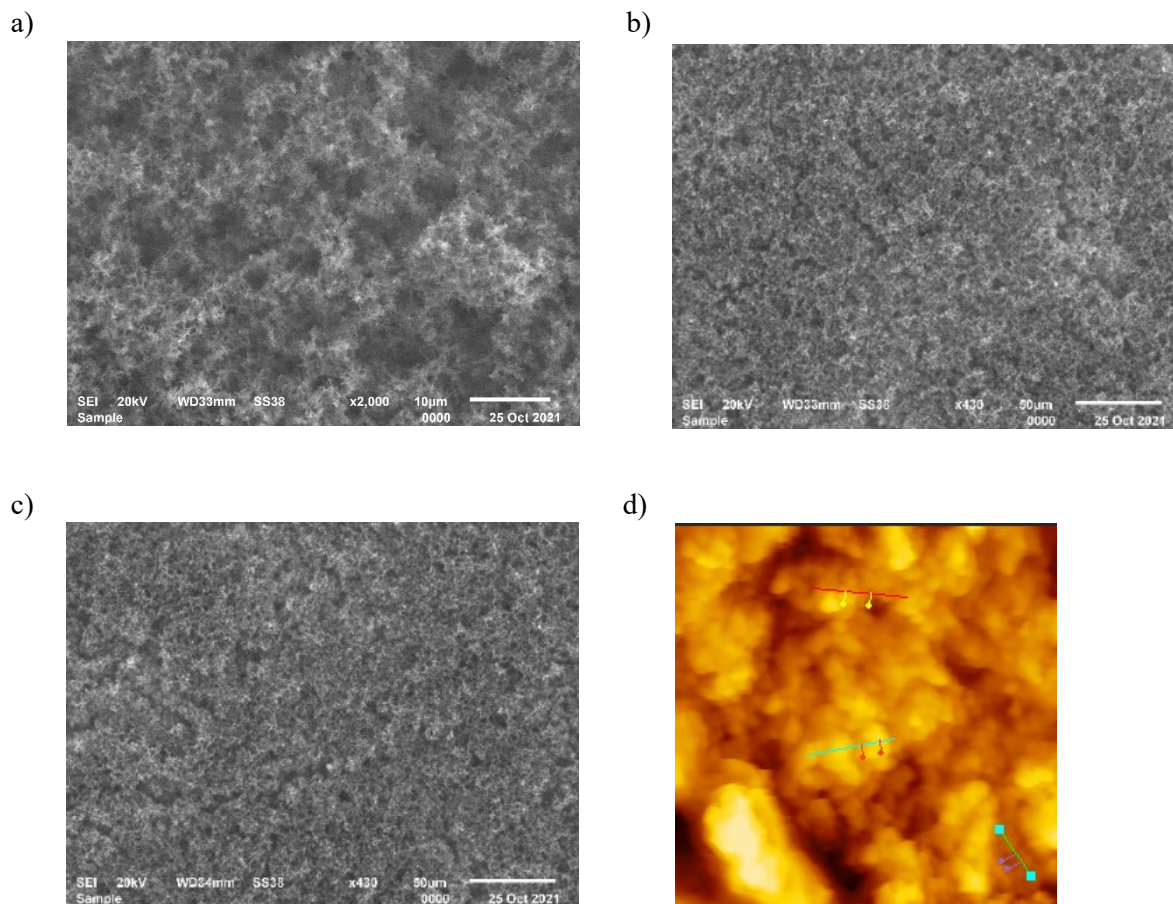


**Figure S6. SEM and AFM images of sensor on ITO glass and gold plate, respectively.** a) Final sensor interface at x2000, b) Final sensor interface at x430, c) Absorption of fentanyl onto the final interface at x430, d) 1.5 μm x 1.5 μm AFM image of final sensor interface

      The morphology of the PANI sensor at various stages of its fabrication was carried out on ITO glass and gold plate. It is observed that there is a largely uniform arrangement of overlapping fibers resulting in a highly porous and sponge-like structure. This porous morphology of PANI benefits sensor sensitivity because the surface area and potential sites of arginine attachment are greatly increased. The surface morphology of PANI does not significantly vary during the steps of fabrication. Fentanyl absorption onto the surface has no noticeable effect on the surface morphology.
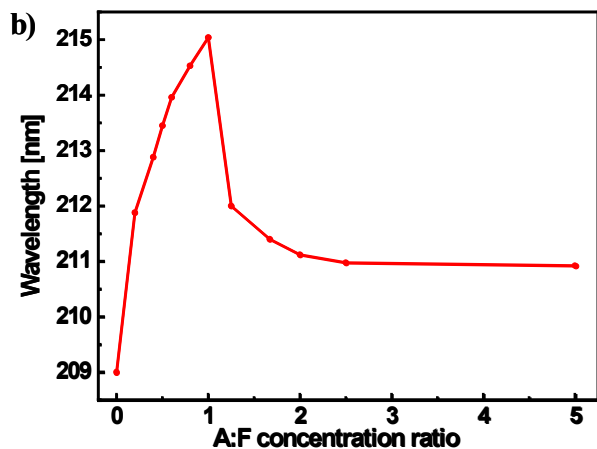
**Figure S7.** The UV absorbance of functional arginine-fentanyl interaction compared with increasing functional arginine (A) to fentanyl (F) ratio.

The interaction of arginine and fentanyl was confirmed using Beckmen Coulter DU-800 UV−vis spectrophotometer. The interaction of arginine towards fentanyl is studied using 0.1mM Fentanyl with varying arginine concentration (0.02 to 0.1mM) in PBS solution. The UV-vis spectrum of the sensor before and after fentanyl detection was studied on ITO (as a working electrode). Further, these interactions were studied using UV absorbance. Adding a small amount of arginine, the absorbance shifts towards longer wavelength, indicating the arginine-fentanyl complex absorbs less energy. This reduces the energy gap of the complex with an increase in delocalization within the molecule. To investigate the interaction between arginine and fentanyl the series of experiments were performed by varying the concentration ratio of arginine to fentanyl. It showed upon increasing arginine content the absorbance shifts to higher wavelength and shifts maximum at 1:1 molar ratio of arginine to fentanyl. This indicates the strong interaction between arginine and fentanyl that helps in the rapid selection of small molecules like fentanyl. On further increase in arginine content results in absorbance shifts back to higher wavelength. This indicates strong arginine-fentanyl complex absorbs more energy resulting from hydrogen bonding between the molecules. Moreover,

interaction between arginine and fentanyl increases the degree of conjugation that increases the delocalization within the complex. These finding from spectroscopy confirms the structural association of AS with fentanyl, which will secure the selectivity of the sensor.
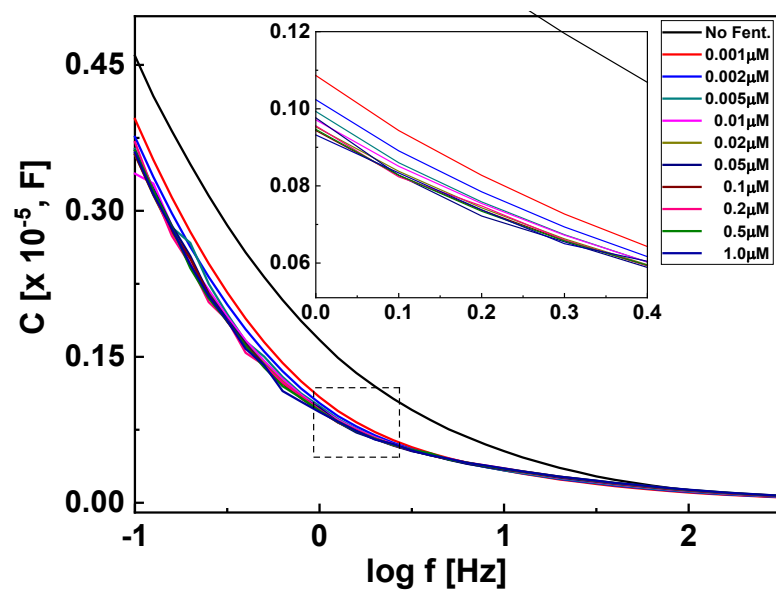
**Supporting Information 4: Sensor Tests**



**Figure S8. Capacitance vs frequency response of the sensor with varying concentration of fentanyl.**

**Supporting Information 4-1 EIS analysis**

The expression of impedance, Z can be written as:

$$Z = \frac{V_t}{I_t} = \frac{V_0 \cdot \sin \omega t}{I_0 \cdot \sin(\omega t + \varphi)} \qquad (S1)$$

where $V_t$ and $I_t$ are the potentials and current at time t, $V_0$ and $I_0$ are the amplitudes of the potential and current, $\omega$ is the angular frequency, and $\Phi$ is the phase angle shift[11, 12]. As can be seen in the above expressions, the impedance is dependent on frequency and phase angle changes at the interface. The impedance (Z) can also be written in the complex form in eq. (2)[11].

$$Z = Z' + jZ'' \qquad (S2)$$

where Z and Z" are dependent on the resistance and capacitive behavior of the material interface. Typically, Z is equivalently contributed by three electrical components of the system: electrolyte and electrode resistance ($R_\Omega$), faradaic impedance ($Z_f$), and capacitance at the interface ($C_i$). These three components can be calculated from the Nyquist plot (Z vs. Z"). Since a very small quantity of fentanyl was being added to the system for this study, the resistance offered by electrolyte and electrode ($R_\Omega$) is negligible. Further, faradaic impedance, $Z_f$ shows no change in recognition as there is no redox reaction occurring during the measurement. Therefore, capacitance ($C_i$) can be an important parameter in molecular recognition for our system. The capacitance can be expressed as eq. (3).[11]

$$\frac{1}{|C_i|} = \frac{1}{\omega |Z|} \qquad (S3)$$

the X-intercept of the Nyquist plot (Z" vs. Z') is not zero for such as modified electrode system, as the modification may introduce the additional resistance or impedance to the electrochemical system. Since our sensing layer structure is stable at the testing condition, both resistance and impedance should keep a constant during the EIS measurement. Z could be considered to discuss and analyze the entire system. Additionally, the impedance Z consists of real part Z' and imaginary part Z'', Z = Z' + jZ''. Similarly, capacitance C, also has C = C' – jC''. Z, Z' and Z'' can be converted to C, C'' and C' by equations[13, 14]:

$$C'(\omega) = \frac{-Z''(\omega)}{\omega |Z(\omega)|^2} \text{ and } C''(\omega) = \frac{Z'(\omega)}{\omega |Z(\omega)|^2}$$

Thus, we will have:

$$C = C' - jC'' = \frac{1}{\omega|Z(\omega)|} \qquad (S4)$$

The presence of fentanyl decreased the surface charge, C, of working electrode by forming cation-$\pi$, H-bond, $\pi$-$\pi$ interactions with AS-PAni. We noticed the phase angle ($\phi$) had a better response to the concentration of fentanyl than any other parameters from EIS measurements, including frequency, Z, Z' and Z''. Therefore, we want to explore the kinetics behind such correlation. From the above analysis, we found that phase angle ($\phi$) is proportional to capacitance (C). Thus, the correlation was established. We noticed the phase angle ($\phi$) had a better sensor response to the concentration of Fentanyl than any other parameters from EIS measurements, including Z, Z' and Z''. Therefore, we want to explore the kinetics behind such correlation.

The fentanyl forms a complex that decreases surface charge by forming cation-$\pi$, H-bond, $\pi$-$\pi$ interactions with AS-PANI. This decrease in surface charge can be seen as a decrease in capacitance at the interface. The decrease in capacitance with the increase in fentanyl concentration can be seen in Figure S8 at intermediate frequencies. This is due to the interaction of fentanyl with AS-PANI decreases the surface charge at the interface with N-H---$\pi$ interaction and stabilizes the complex, thus decreasing the capacitance of the system. The change in capacitance was observed more significantly at lower frequencies than that at intermediate because at lower frequency capacitance represents in maximal capacitance of the system. Moreover, the change in capacitance at higher concentrations is not obvious, so to obtain a better differentiation of fentanyl concentration, phase angle shift was studied for the system. The relation between capacitance and phase angle can be derived from eq. (S1) and (S4) as:

$$Z = \frac{1}{\omega C} = \frac{V_0 \cdot \sin \omega t}{I_0 \cdot \sin (\omega t + \Phi)} \qquad (S5)$$

From equation (S1-5), we found that phase angle ($\phi$) is proportional to capacitance (C). Thus, the correlation was established. Since the phase angle is a parameter that could be directly measured without further analysis. Considering the simplicity of the sensor, here, the phase angles was selected for the sensor application.

Additionally, the EIS data sets were analyzed with ZView software. At this point in time, an equivalent circuit has not been found to truthfully represent the adsorption interface with the functional PANI. We will keep working on this topic and present the results in the future publication.
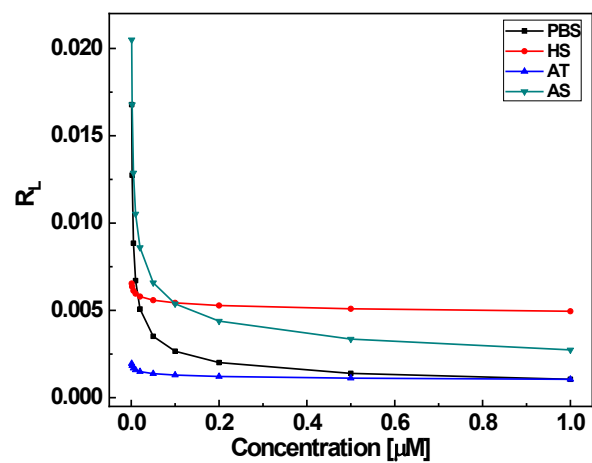
**Figure S9. The nature of fentanyl adsorption on the sensor.** The data were extracted from the figure 3

and S11
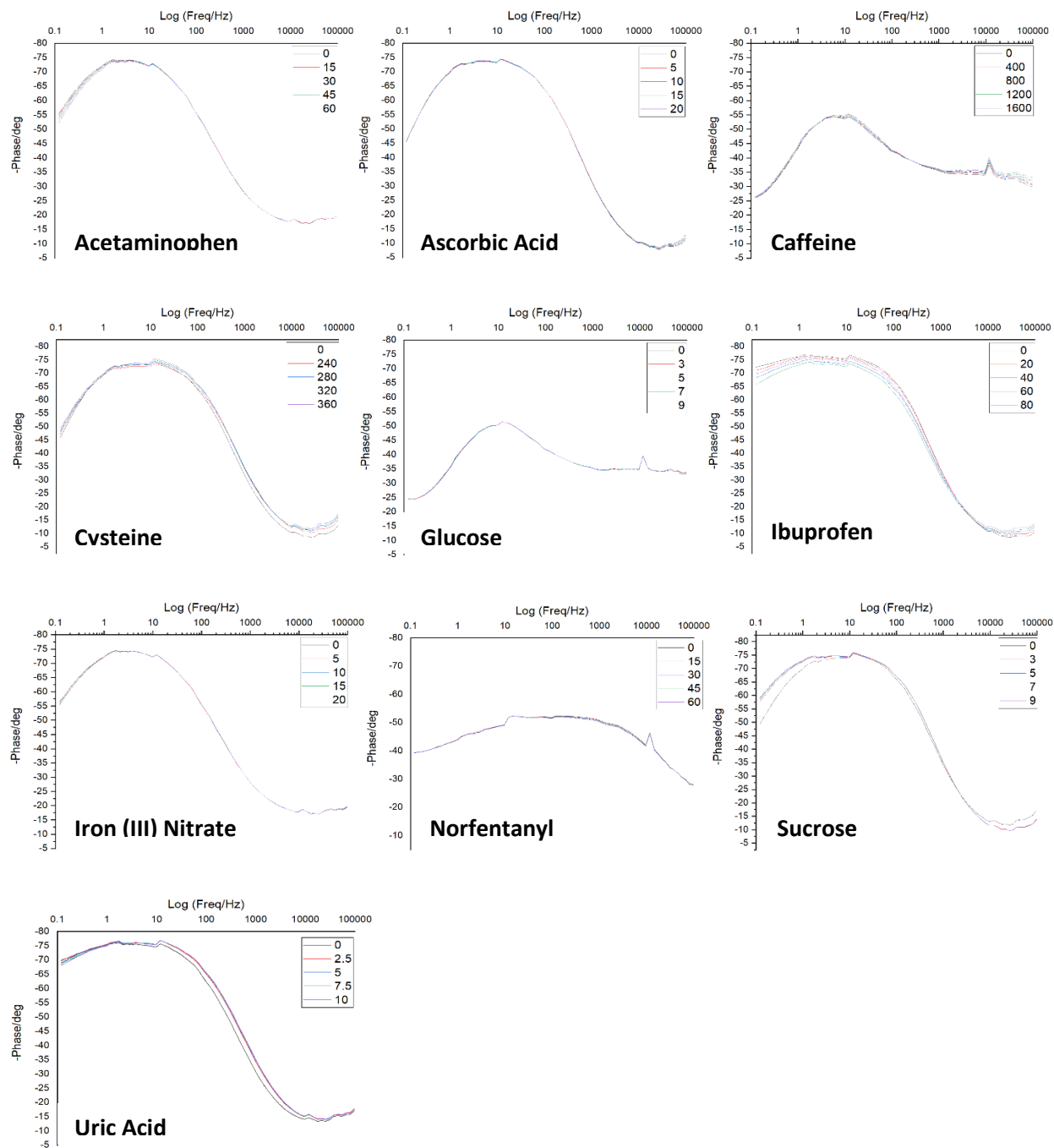
**Figure S10. Selectivity tests of the sensor interface against the interferences**

Electrochemical impedance spectroscopy plots show the sensitivity towards interfering molecules. Molecules were tested in biologically relevant concentrations and in PBS buffer to simulate physiological

conditions. Their respective concentrations are fentanyl (0-90nM), acetaminophen (200-1600 µmol), ascorbic acid (15-60 µmol), caffeine (8-20 µg/mL), cysteine (240-360 µM), glucose (3.9-5.6 mmol), ibuprofen (20-80 µg/mL), iron (III) nitrate (5-20 µM), norfentanyl (15-60 nm), sucrose (3.9-5.6 mmol) and uric acid (2.5-10 mg/dl). Plots indicate that the sensor interface has excellent selectivity towards fentanyl and does not respond to interfering molecules. The following equation was used to calculate the sensitivity of the sensor.

$$Sensitivity \% = \left(\frac{\Delta\varphi\ Interference\ Molecule}{\varphi\ Baseline\ Interference}\right) / \left(\frac{\Delta\varphi\ Fentanyl}{\varphi\ Baseline\ Fentanyl}\right)$$
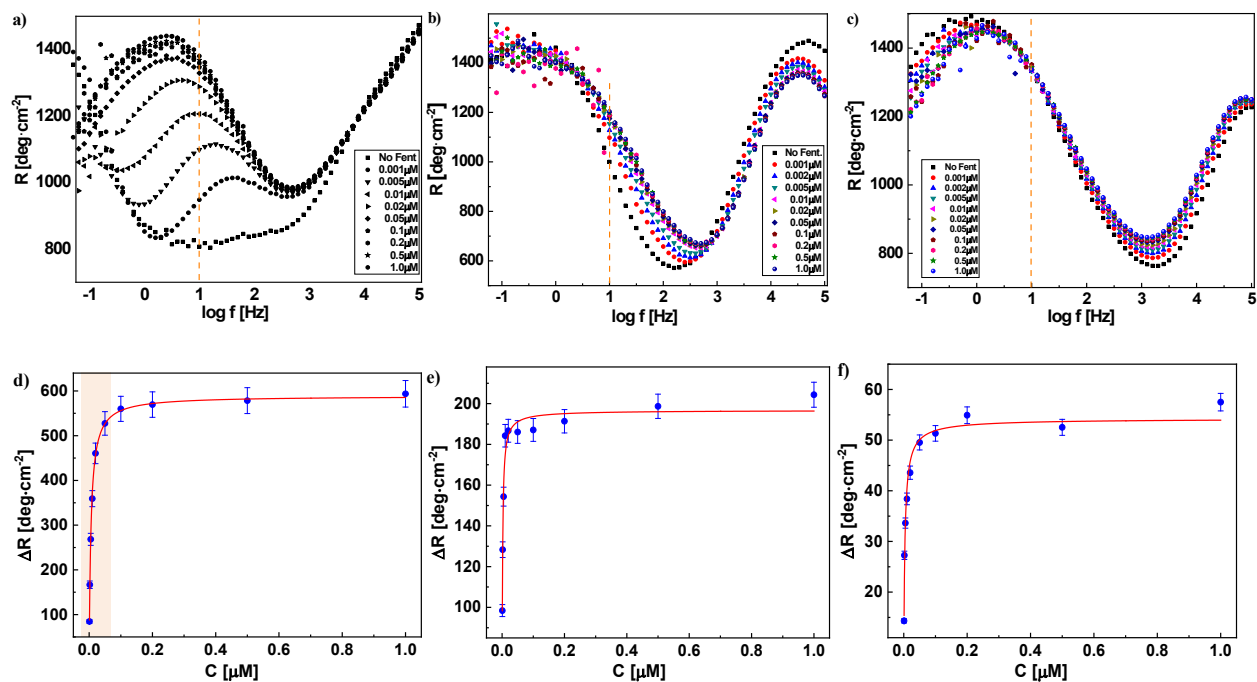
**Figure S11. Sensor calibrations at variable body fluids.** Bode plots and calibration curves in human serum (a & d), artificial tear (b & e), artificial sweat (c & f).

**Table S4. Langmuir parameters obtained after fitting for sensor in different fluids.**

| Langmuir | PBS | HS | AT | AS |
|---|---|---|---|---|
| q | 307.61 | 593.37 | 196.91 | 56.44 |
| kl | 92.60 | 136.72 | 535.37 | 58.79 |
| x | 0.4035 | 0.0405 | 0.0895 | 0.2945 |
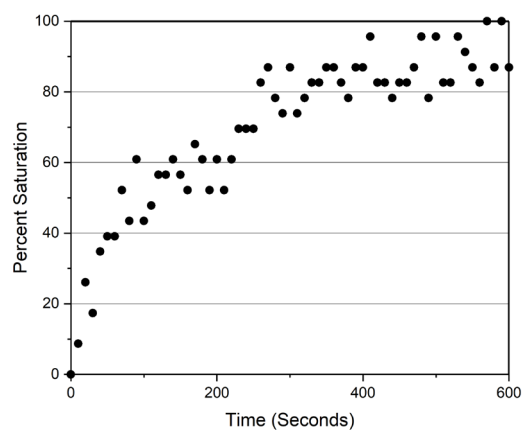
**Figure S12. Saturation of signal upon addition of fentanyl.** Time course measurement of fentanyl absorption onto the sensor. The largest value recorded represents near 100% saturation, with 0% representing the baseline prior to fentanyl addition. Measurements were taken every 2-3 seconds for each and the response was plotted as a function of time.

**Table S5. Current fentanyl detection methods**

| Transducer | EC technique | Linear range | Limit of Detection | Signal response (min) |
|---|---|---|---|---|
| Screen printed carbon electrodes (SPCE) [11] | CSWV | 10-50 µg/mL | | 1 |
| Static Dropping Hg electrode[12] | CV | 0.1-1µM | 0.5nM | After 10min preconcentration |
| Flexible SPCE modified with MWCNTs[13] | SWV | 10-100µM | 10µM | |
| Ru(bpy)$_3$Cl$_2$/GCE[14] | Electrochemiluminescent | 0.1nM-10mM | 8.5nM | |
| *Meta*-aramid fiber wipes[15] | IMS | 1 mg/mL | 1.401ng | |
| Polytetrafluoroethylene coated fiberglass wipes[15] | TD-DART-MS | 1 mg/mL | 0.142ng | |
| *In-house* screen-printed graphite macroelectrodes (SPEs) [16] | HPLC-DAD | 5.0-120 µg/mL | $41.67 \times 10^2$µg/mL | 30 |
| *In-house* screen-printed graphite macroelectrodes (SPEs) [16] | HPLC-AD | 10.0-120 µg/mL | 0.77 µg/mL | 30 |
| PVC membrane electrode[17] | Potentiometric method | 3.36-$3.36 \times 10^3$ µg/mL | 1.83 µg/mL | |
| Plastic membrane electrode (PVC) [18] | Potentiometric method | 3.36-$3.36 \times 10^3$ µg/mL | 2.11 µg/mL | |
| Bond Elute Certify column with helium carrier gas[19] | SPE-GC/MS | $20 \times 10^{-3}$ to $1500 \times 10^{-3}$ µg/mL | $0.4 \times 10^{-3}$ to $4.62 \times 10^{-3}$ µg/mL | 17 |
| Electrospray (ESI) tandem[20] | UPLC-MS/MS | 0.1-1000 pg injected | 0.03-0.21 pg injected | 8 |
| **AS-PANI in this work** (Confidence level at 95%) | Noncovalent pattern-EIS | 5 -1000nM (HS) <br> 3 -1000nM (AT) <br> 9 -200nM (AS) | 12.4 ± 2.1 nM (HS) <br> 11.2 ± 2.0 nM (AT) <br> 9.3 ± 1.8 nM (AS) | <2-3 seconds |

**15-24**
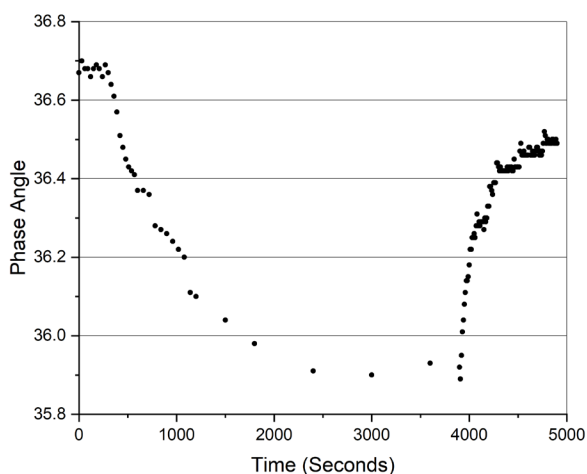
**Figure S13. Time-course measurements of sensor stabilization after two additions of human serum to PBS.** The clinical blood sample testing was performed by add serum sample into PBS in 1: 6 ratio. A series of experiments were performed to evaluate the possible variation from serum vs PBS and serums from different individuals. The results are shown in figure S. At 250th second, the commercial serum sample was added and the phase angle does change upon the absorption of other species from serum. However, it is proportionally a small change (less than 0.8 degrees) in the phase angle, since the mechanism of sensor response is attributed to the electronic structure change of PANI. And further, at 3900th second, a serum sample from another individual was added and showed a different trend than the first one. The phase angle change showed a different direction but was rather small (~0.6 degrees). The result demonstrated the feasibility of testing the serum sample using this method. The different serum sample did not cause such significant impact to the PANI. As a result, testing in a complex environment of human samples does not pose significant challenges when considering the nonspecific absorption of molecules. The patient human sample tests were performed in the commercial serum stabilized PBS solution.

## References for Supporting Information

1.      Grimme, S., Semiempirical hybrid density functional with perturbative second-order correlation. *The Journal of Chemical Physics* **2006,** *124* (3), 034108.

2.      Langreth, D. C.; Mehl, M. J., Beyond the local-density approximation in calculations of ground-state electronic properties. *Physical Review B* **1983,** *28* (4), 1809-1834.

3.      Frisch, M. J.; Trucks, G. W.; Schlegel, H. B.; Scuseria, G. E.; Robb, M. A.; Cheeseman, J. R.; Scalmani, G.; Barone, V.; Petersson, G. A.; Nakatsuji, H.; Li, X.; Caricato, M.; Marenich, A. V.; Bloino, J.; Janesko, B. G.; Gomperts, R.; Mennucci, B.; Hratchian, H. P.; Ortiz, J. V.; Izmaylov, A. F.; Sonnenberg, J. L.; Williams; Ding, F.; Lipparini, F.; Egidi, F.; Goings, J.; Peng, B.; Petrone, A.; Henderson, T.; Ranasinghe, D.; Zakrzewski, V. G.; Gao, J.; Rega, N.; Zheng, G.; Liang, W.; Hada, M.; Ehara, M.; Toyota, K.; Fukuda, R.; Hasegawa, J.; Ishida, M.; Nakajima, T.; Honda, Y.; Kitao, O.; Nakai, H.; Vreven, T.; Throssell, K.; Montgomery Jr., J. A.; Peralta, J. E.; Ogliaro, F.; Bearpark, M. J.; Heyd, J. J.; Brothers, E. N.; Kudin, K. N.; Staroverov, V. N.; Keith, T. A.; Kobayashi, R.; Normand, J.; Raghavachari, K.; Rendell, A. P.; Burant, J. C.; Iyengar, S. S.; Tomasi, J.; Cossi, M.; Millam, J. M.; Klene, M.; Adamo, C.; Cammi, R.; Ochterski, J. W.; Martin, R. L.; Morokuma, K.; Farkas, O.; Foresman, J. B.; Fox, D. J. *Gaussian 16 Rev. C.01*, Wallingford, CT, 2016.

4.      Kassel, L. S., The Limiting High Temperature Rotational Partition Function of Nonrigid Molecules I. General Theory. II. CH4, C2H6, C3H8, CH(CH3)3, C(CH3)4 and CH3(CH2)2CH3. III. Benzene and Its Eleven Methyl Derivatives. *The Journal of Chemical Physics* **1936,** *4* (4), 276-282.

5.      Grimme, S.; Antony, J.; Ehrlich, S.; Krieg, H., A consistent and accurate ab initio parametrization of density functional dispersion correction (DFT-D) for the 94 elements H-Pu. *The Journal of Chemical Physics* **2010,** *132* (15), 154104.

6.      Andzelm, J.; Kölmel, C.; Klamt, A., Incorporation of solvent effects into density functional calculations of molecular energies and geometries. *The Journal of Chemical Physics* **1995,** *103* (21), 9312-9320.

7.      Choi, Y.; Adamczyk, A. J., Tuning Hydrogenated Silicon, Germanium, and SiGe Nanocluster Properties Using Theoretical Calculations and a Machine Learning Approach. *The Journal of Physical Chemistry A* **2018,** *122* (51), 9851-9868.

8.      Adamczyk, A. J.; Cooper, A. C.; Kim, M.-S.; Ivanov, S. V., Leveraging Atomistic Modeling during Precursor Design for Cobalt Film Deposition. In *Computer Aided Chemical Engineering*, Eden, M. R.; Ierapetritou, M. G.; Towler, G. P., Eds. Elsevier: 2018; Vol. 44, pp 157-162.

9.      Minkler, M. J.; Kim, J.; Lawson, K. E.; Ali, A.; Zhao, R.; Adamczyk, A. J.; Beckingham, B. S., Solution processible statistical poly(3-methoxythiophene)-co-poly(3-hexylthiophene) copolymer. *Materials Letters* **2019,** *256*, 126563.

10.     Nautiyal, A.; Cook, J. E.; Zhang, X., Tunable electrochemical performance of polyaniline coating via facile ion exchanges. *Progress in Organic Coatings* **2019,** *136*, 105309.

11.     Orazem, M. E.; Tribollet, B., *Electrochemical Impedance Spectroscopy, 2nd Edition*. 2017; p 768.

12.     Darowicki, K.; Ślepski, P., Dynamic electrochemical impedance spectroscopy of the first order electrode reaction. *JOURNAL OF ELECTROANALYTICAL CHEMISTRY* **2003**.

13.     Orazem, M. E.; Tribollet, B., *Electrochemical Impedance Spectroscopy*. Wiley: 2011.

14.     Taberna, P.; Simon, P.; Fauvarque, J.-F., Electrochemical characteristics and impedance spectroscopy studies of carbon-carbon supercapacitors. *Journal of the Electrochemical Society* **2003,** *150* (3), A292.

15.     Goodchild, S. A.; Hubble, L. J.; Mishra, R. K.; Li, Z.; Goud, K. Y.; Barfidokht, A.; Shah, R.; Bagot, K. S.; McIntosh, A. J. S.; Wang, J., Ionic Liquid-Modified Disposable Electrochemical Sensor Strip for Analysis of Fentanyl. *Anal Chem* **2019,** *91* (5), 3747-3753.

16.     Guo, H.; Hu, N.; Lin, S., Adsorptive stripping voltammetric properties of fentanyl at Hg electrode. *Talanta* **1994,** *41* (11), 1929-32.

17.	Barfidokht, A.; Mishra, R. K.; Seenivasan, R.; Liu, S.; Hubble, L. J.; Wang, J.; Hall, D. A., Wearable electrochemical glove-based sensor for rapid and on-site detection of fentanyl. *Sens Actuators B Chem* **2019,** *296*, 126422.

18.	Dai, H.; Xu, H.; Wu, X.; Chi, Y.; Chen, G., Fabrication of a new electrochemiluminescent sensor for fentanyl citrate based on glassy carbon microspheres and ionic liquid composite paste electrode. *Anal Chim Acta* **2009,** *647* (1), 60-5.

19.	Sisco, E.; Verkouteren, J.; Staymates, J.; Lawrence, J., Rapid detection of fentanyl, fentanyl analogues, and opioids for on-site or laboratory based drug seizure screening using thermal desorption DART-MS and ion mobility spectrometry. *Forensic Chem* **2017,** *4*, 108-115.

20.	Elbardisy, Hadil M.; Foster, C. W.; Cumba, L.; Antonides, L. H.; Gilbert, N.; Schofield, C. J.; Belal, T. S.; Talaat, W.; Sutcliffe, O. B.; Daabees, H. G.; Banks, C. E., Analytical determination of heroin, fentanyl and fentalogues using high-performance liquid chromatography with diode array and amperometric detection. *Analytical Methods* **2019,** *11* (8), 1053-1063.

21.	Peng, L. J.; Wen, M. L.; Yao, Y., Potentiometric determination of fentanyl in pharmaceutical formulations. *J Pharm Biomed Anal* **2002,** *30* (3), 667-73.

22.	Peng, L. J.; Wen, M. L.; Yao, Y., Construction and performance characteristics of new fentanyl-selective plastic membrane electrode. *Anal Sci* **2001,** *17* (7), 815-8.

23.	BRAVO, F.; GONZALEZ, D.; BENITES, J., DEVELOPMENT AND VALIDATION OF A SOLID-PHASE EXTRACTION GAS CHROMATOGRAPHY-MASS SPECTROMETRY METHOD FOR THE SIMULTANEOUS QUANTIFICATION OF OPIOID DRUGS IN HUMAN WHOLE BLOOD AND PLASMA. *Journal of the Chilean Chemical Society* **2011,** *56*, 799-802.

24.	Boleda, M. R.; Galceran, M. T.; Ventura, F., Trace determination of cannabinoids and opiates in wastewater and surface waters by ultra-performance liquid chromatography-tandem mass spectrometry. *J Chromatogr A* **2007,** *1175* (1), 38-48.